



This is a repository copy of *Al0.52In0.48P avalanche photodiodes for soft X-ray spectroscopy*.

White Rose Research Online URL for this paper:

<http://eprints.whiterose.ac.uk/98063/>

Version: Accepted Version

Article:

Auckloo, A., Cheong, J.S., Meng, X. et al. (5 more authors) (2016) Al0.52In0.48P avalanche photodiodes for soft X-ray spectroscopy. *Journal of Instrumentation*, 11 (3). P03021. ISSN 1748-0221

<https://doi.org/10.1088/1748-0221/11/03/P03021>

Reuse

Unless indicated otherwise, fulltext items are protected by copyright with all rights reserved. The copyright exception in section 29 of the Copyright, Designs and Patents Act 1988 allows the making of a single copy solely for the purpose of non-commercial research or private study within the limits of fair dealing. The publisher or other rights-holder may allow further reproduction and re-use of this version - refer to the White Rose Research Online record for this item. Where records identify the publisher as the copyright holder, users can verify any specific terms of use on the publisher's website.

Takedown

If you consider content in White Rose Research Online to be in breach of UK law, please notify us by emailing eprints@whiterose.ac.uk including the URL of the record and the reason for the withdrawal request.

Al_{0.52}In_{0.48}P avalanche photodiodes for soft X-ray spectroscopy

A. Auckloo*, J.S. Cheong, X Meng, C H Tan, J S Ng, A. Krysa, R.C Tozer and J.P.R David

*Department of Electronic and Electrical Engineering, University of Sheffield,
Mappin Street, Sheffield, S1 3JD,
UK*

E-mail: a.auckloo@sheffield.ac.uk

ABSTRACT: The performance of Al_{0.52}In_{0.48}P avalanche photodiodes was assessed as soft X-ray detectors at room temperature. The effect of the avalanche gain improved the energy resolution and an energy resolution (FWHM) of 682 eV is reported for 5.9 keV X-rays.

KEYWORDS: X-ray detectors; spectroscopy; high resolution; low noise.

*Corresponding author.

Contents

1. Introduction	1
2. APD Details	2
3. X-ray measurements	3
3.1 Experiment and method	3
3.2 X-ray spectra	4
4. Discussion	7
5. Conclusion	9

1. Introduction

Detectors without cryogenic cooling are desired in all application due to operational cost. Si based detectors are widely used for X-ray spectroscopy but they have limitations that wide band gap detectors are tackling. Wide band gap compound semiconductors can tolerate harsh environment, particularly high temperature and radiation in some cases. Wide band gap compound semiconductors such as GaAs, SiC and AlGaAs have been investigated for room temperature X-ray detection and comprehensive reviews can be found in [1, 2]. Bertuccio et al. have reported SiC X-ray detectors with sub-keV energy resolution operating in a wide temperature range [3] and some of the best results were achieved with ultra-low noise electronics. SiC detectors with energy FWHM of 315 eV were demonstrated [3], which were later improved to 113 eV [4].

Most of the III-V X-ray research detectors reported in literature are based on GaAs [5–7]. GaAs offers lower leakage current than Ge for instance while providing a better absorption coefficient compared to Si. An energy resolution of 530 eV was reported by Yatsu *et. al* for a Si reach-through Avalanche photodiode at room temperature [8].

The interaction of X-ray photons with a semiconductor detector leads to creation of charges on the electrodes which then appear as current pulses at the detector terminal. For wide bandgap semiconductors, the electron hole pair creation energy is relatively high, resulting into a small amount of electron hole pairs for each absorbed X-ray photon [9]. The total charge created for each absorbed photon can be low, making it challenging to measure. Ultra-low noise electronics, usually a charge sensitive preamplifier, can be used to integrate and amplify the total created charge into a voltage signal in X-ray spectroscopy. The noise performance of the electronics is however improved at the expense of gain. Detecting X-ray less than 10 keV can still be challenging even with low noise electronics as it can be difficult to resolve all the different detected energies or often the detected energies peaks are too close to the noise floor to be resolved. In addition to using ultra-low noise electronics, the internal gain of an Avalanche photodiode (APD) can be used to detect

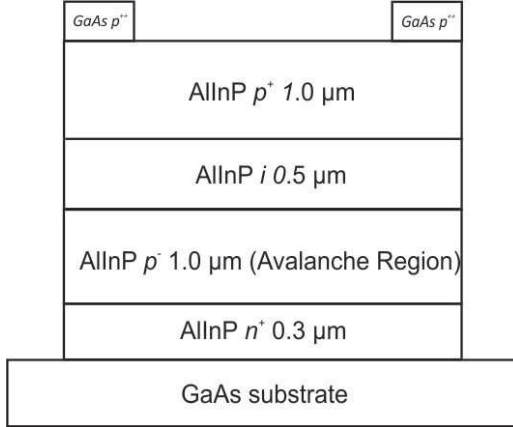


Figure 1. Details of the AlInP APD wafer

and to resolve the different energies peaks for low energy X-rays as the internal gain increases the amount of charge created for each absorbed X-ray photon. The gain from an APD is the end result of successive impact ionization events whereby an energetic electron (or a hole) gives up its energy to create another electron and a hole. The combination of an APD and low noise electronics can, in these cases, provide the gain and the noise performance desired to amplify and pull the detected energies away from the noise floor, thus improving the signal-to-noise ratio.

Gomes et al. have reported a GaAs/Al_{0.8}Ga_{0.2}As Separate Absorption and Multiplication region Avalanche Photodiode (SAM-APD) with a resolution of 1.08 keV when exposed to ⁵⁵Fe source [5]. The effect of avalanche gain improved the resolution.

Al_{0.52}In_{0.48}P is the widest band material that can be grown lattice-matched on a GaAs substrate. Due to its wide bandgap, AlInP can offer reverse dark current of less than 2 pA at gain of 100 for a 200 μm device, making it desirable for room temperature operation[10]. This dark current is limited by surface leakage. In this work, we report a p⁺ – i – p⁻ – n⁺ AlInP APD coupled to an in-house designed low noise charge sensitive amplifier and their characterisation for soft X-ray detection at room temperature. The effects of avalanche gain on the energy resolution of the detected X-ray peak and the noise of the system were experimentally obtained at room temperature.

2. APD Details

The APD used in this work were fabricated from a wafer which, whilst was intended to be a p⁺ – i – p⁻ – n⁺ structure, actually transpired to have a non-uniform p⁻ doping in the 4th layer. This resulted in the structure shown in figure 1. The wafer was grown lattice-matched on a GaAs substrate by Metal Organic Vapour Phase Epitaxy. A highly doped thin 50 nm GaAs cap was grown on the top of the p⁺ AlInP cladding to ensure good ohmic contact. Standard photolithography process and chemical wet-etched were used to fabricate circular mesa diodes with diameters ranging from 50 to 400 μm. To ensure the incident X-ray photons are fully injected from the top AlInP p⁺ cladding layer only, the GaAs cap was etched off, with mesa walls being passivated by SU-8 photoresist. Au/Zn/Au annular contacts were deposited on the top GaAs p⁺ layer of the diode to form ohmic p⁺ contact and the n⁺ contacts were formed by using In/Ge/Au on the substrate. Metal

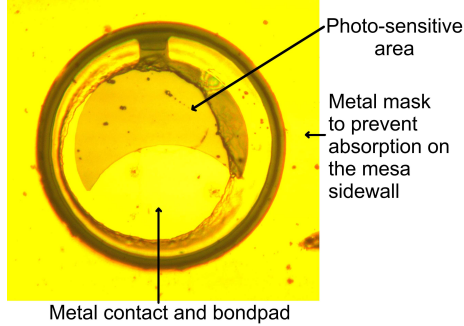


Figure 2. Photograph of one of the 200 μm diameter APDs with bond pad at the top

mask was deposited on the SU-8 to minimise absorption on the mesa side-wall and the bottom n layer. One of the fabricated APDs is shown in figure 2.

Capacitance-Voltage (C-V) measurement was performed on a 200 μm diameter device, shown in figure 3. The minimum voltage required to fully deplete the APD (punch-through voltage) is indicated by the sudden decrease in capacitance at $\sim 41\text{V}$. Between 0 and 41 V, the depletion region exists in the bottom $n^+ - p^-$ junction only. Information of the doping density and thickness of the avalanche region can therefore be deduced from the slope of $d(1/C^2)/dV$ and the values of C, respectively [11]. Beyond this voltage range, the device 'punches-through' with the depletion reaching the top p^+ contact layer. The final capacitance of $\sim 4\text{pF}$ allows the total depletion width of the *i* region and the avalanche region ($1.5\mu\text{m}$) to be estimated. The doping density and thickness of the avalanche region were estimated to be $5.4 \times 10^{16}\text{cm}^{-3}$ and $1.0\mu\text{m}$ respectively. The thickness and doping density of the *i* region was estimated to be $0.5\mu\text{m}$ and $1.5 \times 10^{15}\text{cm}^{-3}$ respectively.

A breakdown voltage of 72 V was obtained in the dark reverse current-voltage (I-V) measurement as illustrated in figure 3. The measured dark current is mainly dominated by surface leakage current prior to avalanche breakdown.

3. X-ray measurements

3.1 Experiment and method

The 200 μm diameter APDs were packaged into TO-5 headers using a gold wire bonder to facilitate X-ray measurements. The TO-5 headers were housed with, and connected to, an in-house low noise charge sensitive amplifier (CSA). The CSA, powered with a $\pm 15\text{V}$ linear power supply, consists of a silicon JFET front-end with an input capacitance of 10 pF followed by a folded cascode configuration. The CSA uses the gate-to-source path of the input JFET to discharge the feedback capacitor, a technique first published by Bertuccio et al. [12]. The CSA's equivalent noise charge is 67 electrons RMS without a detector at the input. The CSA output was connected to an Ortec 570 shaping amplifier (SA) with a shaping time of $0.5\mu\text{s}$. The shaping time of $0.5\mu\text{s}$ was found to achieve the lowest noise in the measurement. The shaping amplifier also provided some voltage gain to the signal from the CSA. The amplified signal was then digitized with an Ortec EasyMCA-8k multichannel analyzer (MCA) interfaced to a computer yielding pulse height spectra.

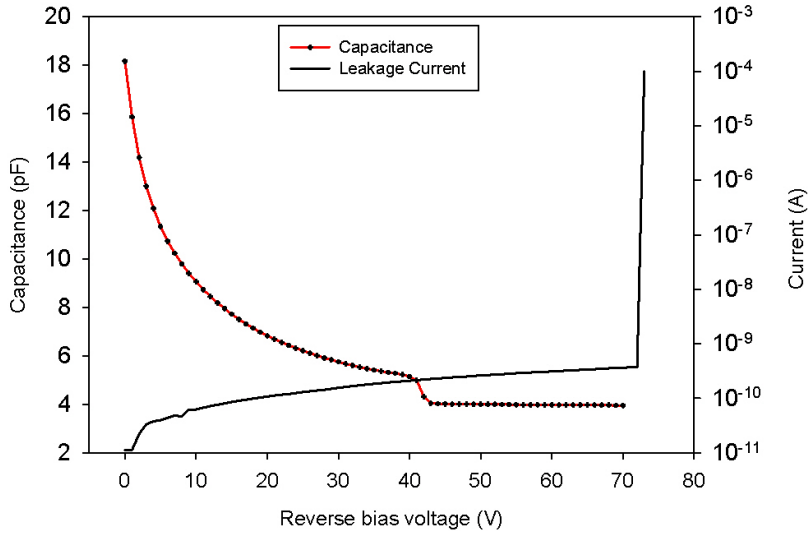


Figure 3. Data of capacitance (left axis) and dark current (right axis) versus reverse bias data of the $200\ \mu\text{m}$ diameter APD

The reverse bias for the APD was applied with a Keithley 2400 Source-Measure unit through a biasing resistor of $330M\Omega$ and a high voltage $10nF$ capacitor to ground. A 55 MBq ^{55}Fe radioisotope source with characteristic Mn K_{α} and K_{β} peaks at 5.9 and 6.49 keV respectively was placed 1 cm away from the APD. Pulse height spectra for different reverse bias voltages were collected at room temperature. For each set of bias voltage, the spectra was collected for a duration of 60 minutes.

3.2 X-ray spectra

Figure 4 (a) and 4 (b) shows the spectra for reverse bias voltage ranging from 15 to 45 V and 45 to 69 V, respectively. Increasing the reverse bias voltage causes the 5.9 keV peak to move away from the noise floor and hence improving the signal-to-noise ratio. The shift of the 5.9 keV peak can be observed more easily in Figure 5, which plots peak position versus reverse bias voltage. The slope of the curve changes gradually with reverse bias voltage, from even the smallest voltage of the data range because of increase in depletion region. For this type of $p^+ - i - p^- - n^+$ structure, at low bias voltage, it is not possible to determine whether the shift of the ^{55}Fe spectral line is due to avalanche gain, M , or increase in carrier collection efficiency.

The higher number of counts registered at bias voltage of 45V indicates that the APD is operating after punch-through ($\sim 41\text{V}$), when the depletion region has widened to include both the $0.5\mu\text{m}$ i-layer and the $1\mu\text{m}$ avalanche region and this increases the charge collection efficiency. Although the increased reverse bias increases M , it also increases the APD leakage current which can in some cases has a detrimental effect on the noise performance.

The Full Width Half Maximum (FWHM) energy resolution of a semiconductor X-ray APD can be expressed as a semi empirical expression from the equations presented in [13, 14], given by:

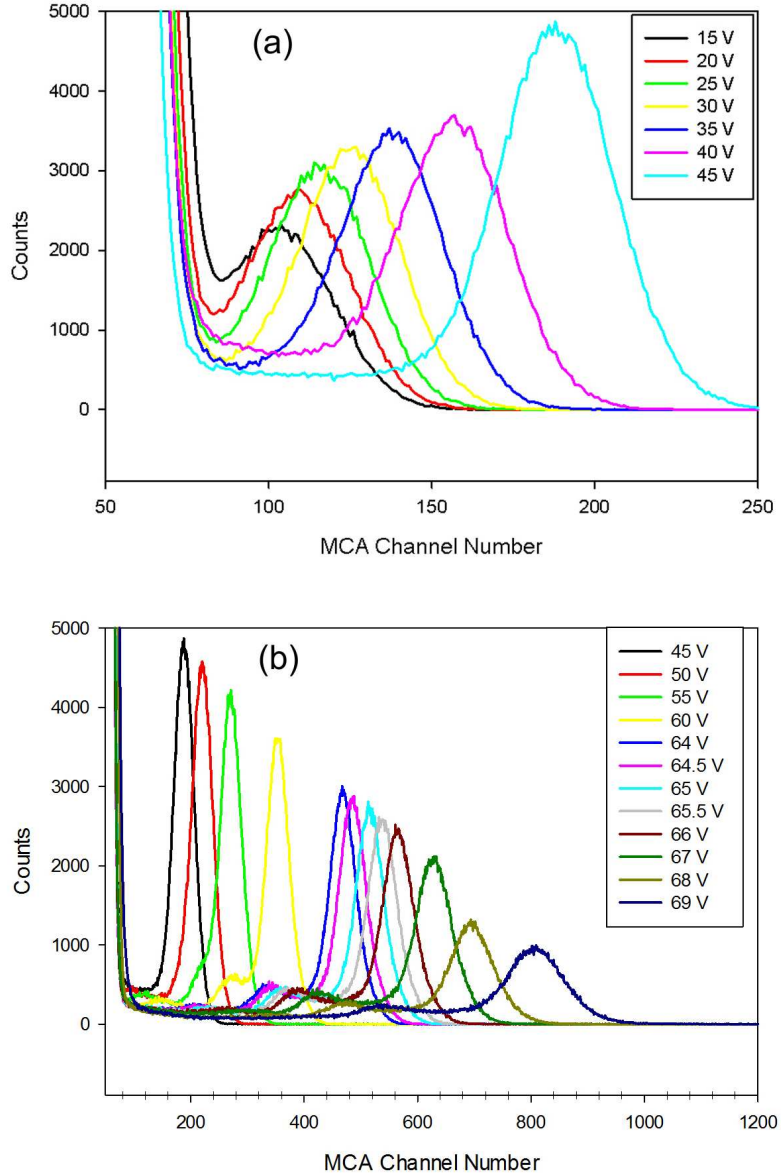


Figure 4. Pulse height spectra collected by the APD, reverse biased at (a) 15 to 45 V, and (b) 45 to 69 V, when irradiated with a ^{55}Fe source

$$(FWHM_{total})^2 = \frac{(2.36\epsilon)^2 (f+F-1) E}{\epsilon} + (FWHM_{EN})^2 \quad (3.1)$$

where f is the Fano factor [15], ϵ is the electron-hole pair creation energy, E is the energy of the incident X-ray, F is the excess noise factor that characterises the gain fluctuation in the APD and $FWHM_{EN}$ accounts for the noise due to the pre-amplifier, detector's leakage current, capacitance and the signal processing.

The total FWHM is usually degraded by $FWHM_{EN}$ and the effect of gain distribution of the

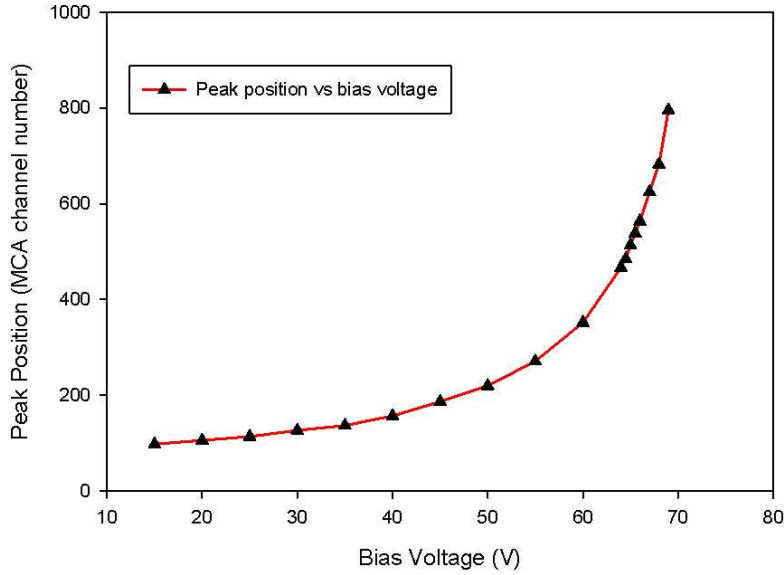


Figure 5. Peak position (in MCA channel number) vs Bias voltage.

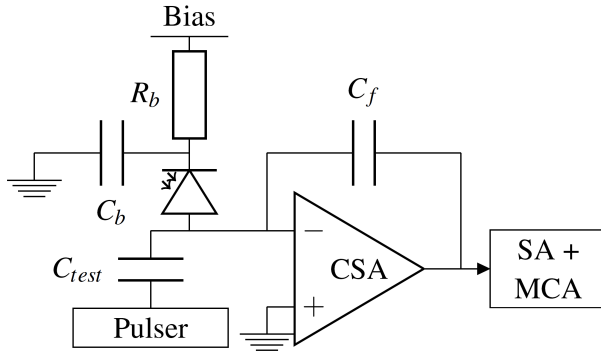


Figure 6. Simplified block diagram of the CSA noise measurement setup

APD if the absorbed photons obey Poissonian statistics (represented by $\frac{(F-1)E}{\epsilon}$ from equation 3.1). For most modern semiconductor crystals, $\frac{(F-1)E}{\epsilon}$ is small compared to $FWHM_{EN}$ [9] and when $\frac{(F-1)E}{\epsilon}$ and $FWHM_{EN}$ are negligible, the spectral resolution is said to be Fano limited. From figure 3, it can be observed that the leakage current of the detector is in the region of 40 pA before breakdown and this is smaller than other research III-V devices presented in literature [16–19]. Thus the contribution of the leakage current of the detector to the term $FWHM_{EN}$ is expected to be small. The contribution of the electronics to the term $FWHM_{EN}$ can be reduced with careful circuit design and a comprehensive analysis of the noise contributions in spectroscopy preamplifiers can be found in [20].

The FWHM of the 5.9 keV energy peak in the collected spectra, with the APD exposed to the

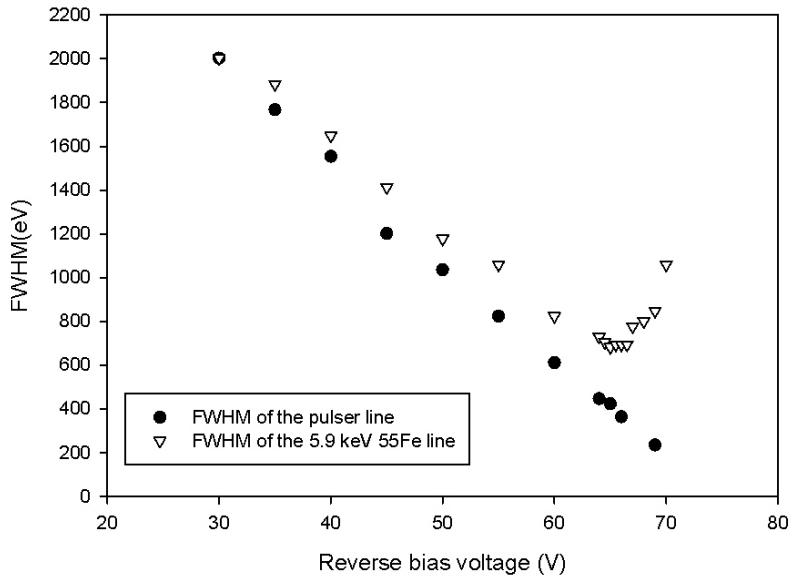


Figure 7. FWHM of the 200 μm diameter APD exposed to ^{55}Fe source and the circuit noise versus reverse bias

^{55}Fe , is used to quantify the energy resolution of the detector spectroscopy system. The channel number information from raw X-ray spectra was converted into energy by using the noise peak and the detected 5.9 keV X-ray peak as references. A Gaussian fitting was then used on 5.9 keV peak in order to determine the FWHM as shown in figure 8. The counts for the energy peak was normalised to facilitate its Gaussian fitting. Secondary peaks is also observed at that bias and their origin is discussed in the next section. Figure 7 shows the experimental FWHM as a function of reverse bias voltage for the collected spectra. The FWHM decreases with increasing reverse bias voltage up to 65 V whereby increasing the bias voltage beyond, leads to an increase of leakage current and hence contributes to an increase in the FWHM.

The noise performance of the system used in this work was assessed using the setup illustrated in figure 6. A pulse generator together with a test capacitor C_{test} was used to simulate charges at the input of the CSA. The pulser line was acquired after the MCA was calibrated using the ^{55}Fe 5.9 keV line obtained for a given bias voltage. The FWHM of the peak produced by the pulse generator was measured to determine the noise contribution of the APD and the electronics, excluding the noise contribution due to fluctuation of the charge generated by absorbed photons since the APD is not exposed to the ^{55}Fe source under those measurements. The measured pulser line FWHM, which includes contribution from the APD leakage current, the CSA, SA and any stray capacitances between the diode and the CSA input, versus bias is presented in figure 7.

The best FWHM from the 5.9 keV X-ray detection was 682 eV at 65V, presented in figure 8. A Gaussian fitting with a standard deviation, σ , of 0.29 is shown.

4. Discussion

The APD internal gain can help to pull the signal away from the electronic noise floor level allow-

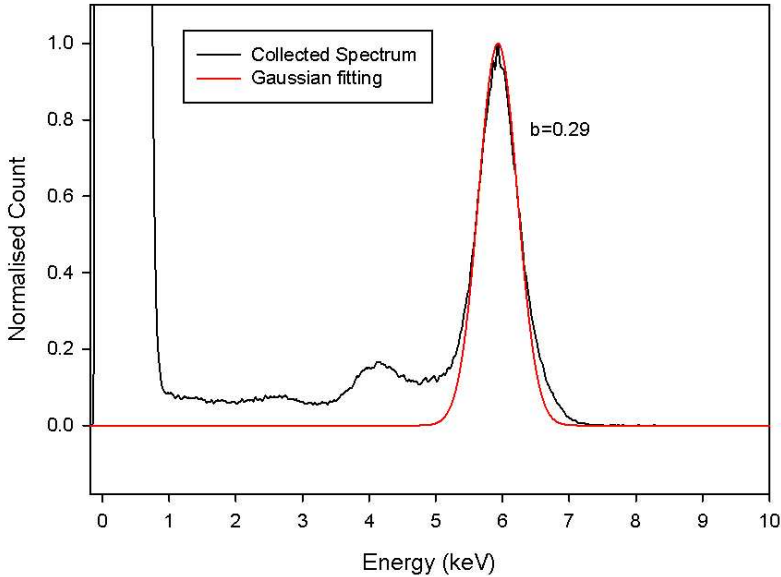


Figure 8. Spectrum collected with an APD reverse biased at 65 V

ing improvement in the measured FWHM energy resolution. Carriers created by absorbed X-ray photons experience avalanche gain, improving the overall signal-to-noise ratio of the system.

Linear absorption coefficient, calculated using data from [21] (weighted average of linear absorption coefficients for each element), was used to define the X-ray photon absorption profile within the device. The absorption of 6 keV X-ray for a total device thickness of $2.8\mu m$ was calculated and it was estimated that 32% of the incident X-ray photons will be absorbed.

When an X-ray photon is absorbed in the diode, a number of electron-hole pairs, dependant on the initial energy of the absorbed photon, are created. The position at which the electron-hole pair is created and the electron (α) and hole (β) ionisation coefficients determines the avalanche multiplication factor M . Photons absorbed in the low field i layer will lead to pure electron initiated multiplication, M_e . For photons absorbed in the n^+ layer, pure hole initiated multiplication, M_h , will occur. Photons absorbed within the p^- (avalanche) region will produce mixed injection. If α is greater than β , electron initiated multiplication will lead to a higher gain than hole initiated multiplication. Hence, holes in the n^+ layer that do undergo impact ionisation, will experience a lower avalanche gain. This will result in two peaks in the spectrum, which moves up the MCA channel number at a different rate with increasing reverse bias.

For bias voltage greater than 50V, a secondary peak is observed in the lower channel numbers. This peak is attributed to X-ray photons that are absorbed in the n^+ cladding or the substrate. Such photons will experience the lower avalanche gain of M_h instead of the higher gain of M_e (the main peak). As the n^+ layer is much thinner than the combined thickness of all the layer above it, fewer electron-hole pairs will be created in that layer making the secondary peak smaller in magnitude compared to the primary peak. As the reverse bias increases, the separation between the two peaks is seen to increase as illustrated in figure 9, because of the increasing difference between the pure electron and pure hole multiplication factors. The relative height of the secondary peak can be

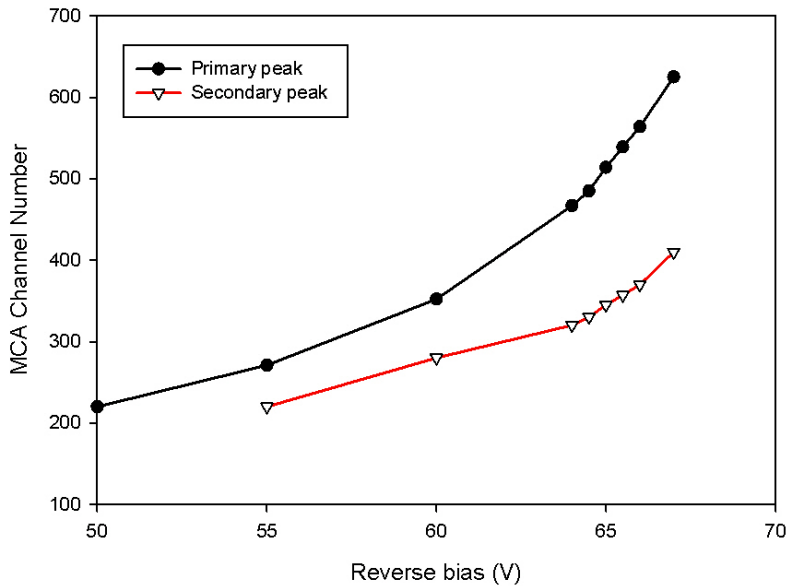


Figure 9. Channel number for primary and secondary peaks versus reverse bias

reduced by increasing the thickness of the i layer, which will also reduce the device capacitance. Dependence of avalanche gain on the carrier injection position for X-ray detectors was clearly illustrated in [22], which pointed out that the secondary peaks are present if electrons and holes have unequal impact ionisation coefficient. The origins of secondary peak for X-ray detectors were also illustrated in [5] for AlGaAs devices.

5. Conclusion

$\text{Al}_{0.52}\text{In}_{0.48}\text{P}$ APDs were demonstrated as soft X-ray photon detector at room temperature. The avalanche gain was shown to move the energy peak away from the noise floor and hence provided higher energy resolution. The best energy resolution (FWHM) of 682 eV was achieved for the 5.9 keV peak. A thicker absorber region would not only reduce the significance of the unwanted secondary peaks in the low channel numbers but also leads to higher detection efficiency.

Acknowledgments

The authors would like to thank Simon Dimler, Researcher at University of Sheffield, for his valuable advice on the optimisation of the setup used in this work.

References

- [1] P. Sellin, *Recent advances in compound semiconductor radiation detectors*, *Nucl. Instrum. Meth. A* **513** (2003) 332.
- [2] D. McGregor and H. Hermon, *Room-temperature compound semiconductor radiation detectors*, *Nucl. Instrum. Meth. A* **395** (1997) 101.

- [3] G. Bertuccio, R. Casiraghi, A. Cetronio, C. Lanzieri, and F. Nava, *Silicon carbide for high resolution X-ray detectors operating up to 100°C*, *Nucl. Instrum. Meth. A* **552** (2004) 413.
- [4] G. Bertuccio, S. Caccia, D. Puglisi, and D. Macera, *Advances in silicon carbide x-ray detectors*, *Nuclear Instruments and Methods in Physics Research Section A: Accelerators, Spectrometers, Detectors and Associated Equipment* **652** (2011), no. 1 193 – 196. Symposium on Radiation Measurements and Applications (SORMA) {XII} 2010.
- [5] R. B. Gomes, C. H. Tan, X. Meng, J. P. R. David, and J. S. Ng, *GaAs/Al_{0.8}Ga_{0.2}As avalanche photodiodes for soft X-ray spectroscopy*, *Journal of Instrumentation* **9** (2014), no. 03 P03014.
- [6] G. Bertuccio, A. Pullia, J. Lauter, A. Forster, and H. Luth, *Pixel X-ray detectors in epitaxial gallium arsenide with high-energy resolution capabilities (Fano factor experimental determination)*, *Nuclear Science, IEEE Transactions on* **44** (Feb, 1997) 1–5.
- [7] G.C. Sun and N. Manez and J.C. Bourgoin, *X-ray detectors made of self-supported epitaxial gaas*, *Nuclear Instruments and Methods in Physics Research Section A: Accelerators, Spectrometers, Detectors and Associated Equipment* **563** (2006), no. 1 13 – 16.
- [8] Y. Yatsu, Y. Kuramoto, J. Kataoka, J. Kotoku, T. Saito, T. Ikagawa, R. Sato, N. Kawai, S. Kishimoto, K. Mori, T. Kamae, Y. Ishikawa, and N. Kawabata, *Study of avalanche photodiodes for soft X-ray detection below 20 keV*, *Nuclear Instruments and Methods in Physics Research Section A: Accelerators, Spectrometers, Detectors and Associated Equipment* **564** (2006), no. 1 134 – 143.
- [9] A. Owens and A. Peacock, *Compound semiconductor radiation detectors*, *Nuclear Instruments and Methods in Physics Research* **531** (2004), no. 1 - 2 18 – 37.
- [10] J. S. Cheong, J. Ong, J. S. Ng, A. Krysa, and J. P. R. David, *Al_{0.52}In_{0.48}P SAM-APD as a Blue-Green Detector*, *IEEE Journal of Selected Topics in Quantum Electronics* **20** (Nov, 2014) 142–146.
- [11] S. Sze and K. K. Ng, *p-n Junctions*, pp. 77–133. John Wiley & Sons, Inc., 2006.
- [12] G. Bertuccio, P. Rehak, and D. Xi, *A novel charge sensitive preamplifier without the feedback resistor*, *Nuclear Instruments and Methods in Physics Research* **326** (1993) 71–76.
- [13] L. M. P. Fernandes, F. D. Amaro, A. Antognini, J. M. R. Cardoso, C. A. N. Conde, O. Huot, P. E. Knowles, F. Kottmann, J. A. M. Lopes, L. Ludhova, C. M. B. Monteiro, F. Mulhauser, R. Pohl, J. M. F. dos Santos, L. A. Schaller, D. Taqqu, and J. F. C. A. Veloso, *Characterization of large area avalanche photodiodes in x-ray and vuv-light detection*, *Journal of Instrumentation* **2** (2007), no. 08 P08005.
- [14] G. Knoll, *Radiation Detection and Measurement*. Wiley, 2000.
- [15] U. Fano, *Ionization yield of radiations. II. the fluctuations of the number of ions*, *Phys. Rev.* **72** (Jul, 1947) 26–29.
- [16] B. Li, Q.-Q. Lv, R. Cui, W.-H. Yin, X.-H. Yang, and Q. Han, *A Low Dark Current Mesa-Type InGaAs/InAlAs Avalanche Photodiode*, *Photonics Technology Letters, IEEE* **27** (Jan, 2015) 34–37.
- [17] M. Achouche, G. Glastre, C. Caillaud, M. Lahrichi, M. Chtioui, and D. Carpentier, *InGaAs Communication Photodiodes: From Low- to High-Power-Level Designs*, *Photonics Journal, IEEE* **2** (June, 2010) 460–468.
- [18] M. Lahrichi, E. Derouin, D. Carpentier, N. Lagay, J. Decobert, G. Glastre, and M. Achouche, *Very low dark current AlInAs/GaInAs SAGM avalanche photodiodes for 10Gb/s applications*, in *Optical Communication, 2009. ECOC '09. 35th European Conference on*, pp. 1–2, Sept, 2009.

- [19] D. Franco, K. Vaccaro, W. Clark, W. Teynor, H. M. Dauplaise, M. Roland, B. Krejca, and J. P. Lorenzo, *High-performance InGaAs-InP APDs on GaAs*, *Photonics Technology Letters, IEEE* **17** (April, 2005) 873–874.
- [20] G. Bertuccio, A. Pullia, and G. D. Geronimo, *Criteria of choice of the front-end transistor for low-noise preamplification of detector signals at sub-microsecond shaping times for X- and γ -ray spectroscopy*, *Nuclear Instruments and Methods in Physics Research* **380** (1996), no. 1 - 2 301 – 307.
- [21] J. H. Hubbell and S. M. Seltzer, *Tables of X-Ray Mass Attenuation Coefficients and Mass Energy-Absorption Coefficients*, National Institute of Standards and Technology (July, 2004).
- [22] C. H. Tan, R. B. Gomes, J. P. R. David, A. M. Barnett, D. J. Bassford, J. E. Lees, and J. S. Ng, *Avalanche gain and energy resolution of semiconductor X-ray detectors*, *IEEE Trans. Electron Dev.* **58** (2011) 1696.